Macroscopic electrostatic stability properties of nonrelativistic non-neutral electron flow in a cylindrical diode with applied magnetic field

Ronald C. Davidson
Plasma Fusion Center, Massachusetts Institute of Technology, Cambridge, Massachusetts 02139

Kang Tsang
Science Applications, Inc., Boulder, Colorado 80302

(Received 6 October 1983)

Electrostatic stability properties of nonrelativistic non-neutral electron flow in a cylindrical diode with applied magnetic field $B_0\hat{e}_z$ are investigated within the framework of the macroscopic cold-fluid-Poisson equations. The electrostatic eigenvalue equation is derived for perturbations about the general class of slow rotational equilibria with angular velocity profile $\omega_b^-(r)=V_{\theta b}^0(r)/r=(\omega_c/2)\{1-[1-(4/\omega_c^2 r^2)\int_a^r dr'r'\omega_{pb}^2(r')]^{1/2}\}$. Here, $\omega_c=eB_0/mc$, $\omega_{pb}^2(r)=4\pi n_b^0(r)e^2/m$, $n_b^0(r)$ is the equilibrium electron density profile, and the cathode is located at $r=a$ and the anode at $r=b$. Space-charge-limited flow is assumed with $E_r^0(r=a)=0$ and $\phi^0(r=a)=0$. The exact eigenvalue equation is simplified for low-frequency flute perturbations with $k_z=0$ and $|\omega-l\omega_b^-(r)|^2 \ll \omega_c^2-\omega_{pb}^2(r)$, assuming $\omega_{pb}^2(r)<\omega_c^2$ and a moderate-aspect-ratio diode ($R_0 \gg b-a$). In this regime, it is shown that $\partial n_b^0/\partial r \leq 0$ over the interval $a \leq r \leq b$ is a *sufficient condition for stability*, and specific examples of stable oscillations (rectangular density profile) and weak resonant diocotron instability (gentle density bump) are analyzed in detail. Finally, the exact eigenvalue equation is solved numerically for a wide range of density profiles $n_b^0(r)$ and values of $\omega_{pb}^2(r)/\omega_c^2$ leading to weak and strong instability driven by velocity shear with $\partial\omega_b^-(r)/\partial r \neq 0$.

I. INTRODUCTION AND SUMMARY

The use of high-voltage diodes to generate intense charged particle beams for inertial-confinement fusion applications[1-4] has resulted in a concomitant need for a better theoretical understanding of the equilibrium and stability properties of non-neutral electron flow in various diode configurations. While there is a growing literature[5-13] on the equilibrium and stability properties of non-neutral plasmas based on the Vlasov-Maxwell equations, it is often difficult in a kinetic treatment to obtain detailed estimates of instability growth rates, primarily because of the complications introduced by strong spatial inhomogeneities and intense self-generated fields. Therefore, in the present analysis, we investigate the stability properties of non-neutral electron flow in a cylindrical diode making use of a macroscopic cold-fluid model[14-25] for the electrons. The stability analysis is electrostatic and assumes nonrelativistic laminar electron flow. However, the present formalism can be extended in a relatively straightforward manner to include the electromagnetic and relativistic effects.[24]

In a recent calculation,[15] we made use of global conservation constraints satisfied by the fully nonlinear Vlasov-Maxwell equations to derive a sufficient condition for stability of the class of self-consistent planar diode equilibria $f_b^0(H-V_bP_y)$, where $V_b=$const. In the present analysis, we make use of a *macroscopic, cold-fluid* model (Secs. II and III) to investigate *electrostatic* stability properties of *nonrelativistic* sheared electron flow in a cylindrical diode with strong applied axial magnetic field $B_0\hat{e}_z$ (Fig. 1). After reviewing the cold-fluid equilibrium properties, the linearized fluid-Poisson equations (25)–(27) are used in Sec. III to investigate stability behavior for electrostatic perturbations about a non-neutral cylindrical equilibrium characterized by (general) electron density profile $n_b^0(r)$ and self-consistent azimuthal velocity profile $V_{\theta b}^0(r)=\omega_b^-(r)r$ defined in terms of $n_b^0(r)$ in Eq. (15). Here, the cathode is located at $r=a$, and the anode at

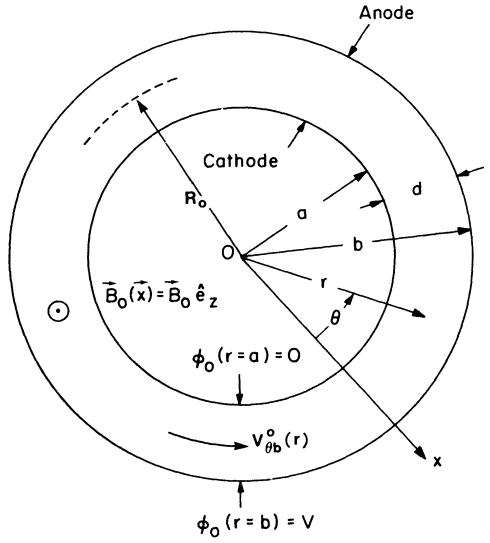

FIG. 1. Cylindrical diode configuration with cathode at $r=a$ and anode at $r=b$, and applied axial magnetic field $\vec{B}_0(\vec{x})=B_0\hat{e}_z$. Equilibrium electron flow is in the θ direction.

$r=b$ (Fig. 1). Moreover, $\omega_c=eB_0/mc$ is the (nonrelativistic) electron cyclotron frequency, and $\omega_{pb}^2(r)=4\pi n_b^0(r)e^2/m$ is the electron plasma frequency, squared. For perturbations with complex oscillation frequency $\omega=\omega_r+i\gamma$, axial wave number k_z, and azimuthal harmonic number l [Eq. (28)], the linearized fluid-Poisson equations (29)—(33) can be combined to give [Eq. (34)],

$$\frac{1}{r}\frac{\partial}{\partial r}\left[r\left[1-\frac{\omega_{pb}^2}{\nu_b^2}\right]\frac{\partial}{\partial r}\delta\phi^l\right]-\frac{l^2}{r^2}\left[1-\frac{\omega_{pb}^2}{\nu_b^2}\right]\delta\phi^l - k_z^2\left[1-\frac{\omega_{pb}^2}{(\omega-l\omega_b^-)^2}\right]\delta\phi^l = -\frac{l\delta\phi^l}{r}\frac{1}{(\omega-l\omega_b^-)}\frac{\partial}{\partial r}\left[\frac{\omega_{pb}^2}{\nu_b^2}(2\omega_b^- -\omega_c)\right] .$$

Here, $\delta\phi^l(k_z,r)$ is the perturbed electrostatic potential, $\omega_{pb}^2(r)=4\pi n_b^0(r)e^2/m$, $\omega_c=eB_0/mc$, and $\nu_b^2(r)=[\omega-l\omega_b^-(r)]^2-[\omega_c^2-\omega_{pb}^2(r)-2\omega_c\omega_E(r)]$, where $\omega_E(r)=-cE_r^0(r)/B_0r$.

The eigenvalue equation (34) provides an exact cold-fluid description of electrostatic stability properties, assuming nonrelativistic electron flow. For a moderate-aspect-ratio diode with $d\ll a$ (Fig. 1), it follows that $\omega_E(r)\ll\omega_c$ [Eq. (39)], and the eigenvalue equation (34) further simplifies to give the approximate eigenvalue equation in Eq. (43). In Secs. IV and VI, we analyze Eq. (43) for the special case of low-frequency flute perturbations with $k_z=0$, and $|\omega-l\omega_E(r)|^2\ll\omega_c^2-\omega_{pb}^2(r)$, assuming that the electron density is below the condition for Brillouin flow, i.e., $\omega_{pb}^2(r)<\omega_c^2$. In this case, the eigenvalue equation (43) can be approximated by Eq. (47). In Sec. IV A, we make direct use of the eigenvalue equation (47) to show that $\partial\omega_{pb}^2(r)/\partial r\le 0$ over the interval $a\le r\le b$ is a sufficient condition to assure electrostatic stability [Eq. (55)]. That is, equilibrium density profiles that decrease monotonically from the cathode to the anode are electrostatically stable. For the special case of weak resonant diocotron instability with growth rate $\gamma=\mathrm{Im}\omega\ll|\omega_r|$, a formal expression for the growth rate γ is derived in Eq. (60) of Sec. IV B, where $\omega_r=\mathrm{Re}\omega$ is determined from the dispersion relation (59). In Sec. V, analytic solutions to the electrostatic eigenvalue equation (47) are determined both for the stable surface modes on an annular electron beam (Sec. V A), and for weak resonant diocotron instability driven by a small density bump with $\partial\omega_{pb}^2/\partial r|_{r=r_s}>0$ (Sec. V B).

Because of the very general nature of the stability theorem obtained directly from the eigenvalue equation (47), we have also developed an *indirect* proof that $\partial n_b^0/\partial r\le 0$ is a sufficient condition for electrostatic stability.[25] The analysis in Ref. 25 is based on a cold-fluid guiding-center model in which electron inertial effects are neglected ($m\to 0$ and $B_0\to\infty$) and the motion of an electron fluid element is determined from $\vec{V}_b=(-c/B_0)\vec{\nabla}\phi\times\hat{e}_z$. Making use of exact global conservation constraints, it is shown that $\partial n_b^0/\partial r\le 0$ over the interval $a\le r\le b$ is a sufficient condition for electrostatic stability to small-amplitude perturbations.

Finally, in Sec. VI we solve numerically the exact electrostatic eigenvalue equation (34) for $k_z=0$ and a wide range of electron density profiles $n_b^0(r)$ leading to weak and strong instability driven by velocity shear. In this regard, it should be emphasized that the exact eigenvalue equation (34) fully includes cylindrical effects and the influence of finite aspect ratio. Moreover, Eq. (34) allows for arbitrary values of $\omega_{pb}^2(r)/\omega_c^2$ consistent with the existence of radially confined equilibria. Therefore, in the numerical analysis of Eq. (34) presented in Sec. VI, no *a priori* restriction has been made to planar geometry[16,20,22–24] or to low electron density with $\omega_{pb}^2\ll\omega_c^2$.[15,17,18,20,21,25]

II. LAMINAR COLD-FLUID EQUILIBRIUM FOR A CYLINDRICAL DIODE

A. Theoretical model and assumptions

We consider here the equilibrium properties ($\partial/\partial t=0$) for a cold, non-neutral pure electron plasma confined in the cylindrical diode configuration illustrated in Fig. 1. The cathode is located at $r=a$ and the anode at $r=b$, where $d=b-a$ is the anode-cathode spacing. In addition, the electron fluid is immersed in a uniform applied magnetic field $B_0\hat{e}_z$. The equilibrium analysis is based on a macroscopic cold-fluid description with the following simplifying assumptions:

(i) The electron fluid is uniform in the z direction, with $\partial n_b^0(\vec{x})/\partial z=0$ and $\partial\vec{V}_b^0(\vec{x})/\partial z=0$, and there is no equilibrium electric field parallel to $B_0\hat{e}_z$, i.e., $\vec{E}^0(\vec{x})\cdot\hat{e}_z=0$.

(ii) The equilibrium radial density profile and the azimuthal flow velocity profile are assumed to be azimuthally symmetric, i.e.,

$$n_b^0(\vec{x})=n_b^0(r) , \qquad \vec{V}_b^0(\vec{x})=V_{\theta b}^0(r)\hat{e}_\theta , \tag{1}$$

where r is the radial distance from the axis of symmetry, and $\hat{e}_\theta$ and $\hat{e}_z$ are unit vectors in the θ and z directions, respectively. The equilibrium continuity equation $\vec{\nabla}\cdot[n_b^0(\vec{x})\vec{V}_b^0(\vec{x})]=0$ is automatically satisfied for general profiles $n_b^0(r)$ and $V_{\theta b}^0(r)$.

(iii) The azimuthal current $J_\theta^0(r)=-en_b^0(r)V_{\theta b}^0(r)$ will generally induce an axial self-magnetic field $B_z^s(r)$. Throughout the present analysis, it is assumed that the azimuthal current is sufficiently weak that the axial self-magnetic field is negligibly small in comparison with the applied magnetic field, i.e.,

$$|B_z^s(r)|\ll B_0 . \tag{2}$$

(iv) The electron fluid is assumed to be sufficiently cold that pressure gradients can be neglected in the equilibrium force balance equation, i.e.,

$$\frac{\partial}{\partial\vec{x}}\cdot\vec{P}_b^0=0 . \tag{3}$$

It is convenient to introduce the notation

$$V_{\theta b}^0(r)=\omega_b(r)r , \tag{4}$$

in the subsequent analysis. Within the context of assumptions (i)—(iii), the equilibrium field components are

$$\vec{E}_0(\vec{x})=E_r^0(r)\hat{e}_r\ ,$$
$$\vec{B}_0(\vec{x})=B_0\hat{e}_z\ , \tag{5}$$

where the electric field is determined from the steady-state Poisson equation

$$\frac{1}{r}\frac{\partial}{\partial r}[rE_r^0(r)]=-4\pi e n_b^0(r)\ , \tag{6}$$

and $-e$ is the electron charge. Integrating Eq. (6) gives the equilibrium radial electric field

$$E_r^0(r)=-\frac{4\pi e}{r}\int_0^r dr'\,r'n_b^0(r')\ , \tag{7}$$

where space-charge-limited flow with

$$E_r^0(r=a)=0 \tag{8}$$

is assumed. We introduce the electrostatic potential $\phi_0(r)$, where $E_r^0=-\partial\phi^0/\partial r$, and impose the boundary conditions

$$\phi_0(r=a)=0\ ,$$
$$\phi_0(r=b)=V\ . \tag{9}$$

The anode voltage V consistent with Eqs. (7) and (8) is given by

$$V=\phi_0(b)=4\pi e\int_a^b\frac{dr''}{r''}\int_a^{r''}dr'\,r'n_b^0(r')\ . \tag{10}$$

(v) Finally, for analytic simplicity, it is assumed in the present analysis that the fluid motion is nonrelativistic. In equilibrium, radial force balance on a fluid element can therefore be expressed as

$$\frac{-m[V_{\theta b}^0(r)]^2}{r}=-e\left[E_r^0(r)+\frac{1}{c}V_{\theta b}^0(r)B_0\right]\ . \tag{11}$$

B. Equilibrium flow properties

Substituting Eqs. (4) and (7) into Eq. (11) gives (for $a\le r\le b$)

$$\omega_b^2(r)-\omega_b(r)\omega_c+\frac{1}{r^2}\int_a^r dr'\,r'\omega_{pb}^2(r')=0\ , \tag{12}$$

where

$$\omega_c=\frac{eB_0}{mc}\quad\text{and}\quad\omega_{pb}^2(r)=\frac{4\pi e^2n_b^0(r)}{m} \tag{13}$$

are the (nonrelativistic) cyclotron frequency and plasma frequency, squared. Solving Eq. (12) for the angular velocity profile $\omega_b(r)$ gives[14]

$$\omega_b(r)=\omega_b^{\pm}(r)$$
$$=\frac{\omega_c}{2}\left[1\pm\left[1-\frac{4}{\omega_c^2r^2}\int_a^r dr'\,r'\omega_{pb}^2(r')\right]^{1/2}\right]\ . \tag{14}$$

Note from Eq. (14) that there are *two* allowed equilibrium rotation frequencies, with $\omega_b^+(r)$ corresponding to a *fast*-rotational equilibrium, and $\omega_b^-(r)$ corresponding to a *slow*-rotational equilibrium. Note also from Eq. (14) that $\omega_b^-(r=a)=0$ at the cathode, whereas $\omega_b^+(r=a)=\omega_c$. In the subsequent equilibrium and stability analysis, it is assumed that

$$V_{\theta b}^0(r)=\omega_b^-(r)r$$
$$=\frac{r\omega_c}{2}\left[1-\left[1-\frac{4}{\omega_c^2r^2}\int_a^r dr'\,r'\omega_{pb}^2(r')\right]^{1/2}\right]\ , \tag{15}$$

corresponding to a *slow*-rotational equilibrium. In the special case where

$$\frac{4}{r^2\omega_c^2}\int_a^r dr'\,r'\omega_{pb}^2(r')\ll 1\ , \tag{16}$$

Eq. (15) can be approximated

$$V_{\theta b}^0(r)=\frac{1}{\omega_c r}\int_a^r dr'\,r'\omega_{pb}^2(r')=-\frac{cE_r^0(r)}{B_0}\ , \tag{17}$$

corresponding to an $\vec{E}_0(\vec{x})\times B_0\hat{e}_z$ equilibrium rotation of a fluid element. In general, however, centrifugal effects should also be retained in Eq. (11), which gives the expression for $V_{\theta b}^0(r)$ in Eq. (15).

From Eq. (15), $\omega_b^-(r)$ can be determined for a broad class of equilibrium density profiles $n_b^0(r)$. By way of illustration, consider the rectangular density profile [Fig. 2(a)] specified by

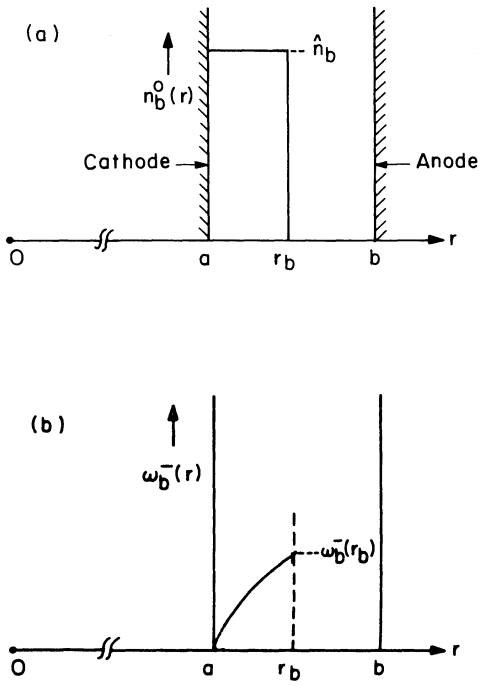

FIG. 2. (a) Rectangular density profile $n_b^0(r)$ assumed in Eq. (18). (b) Corresponding angular velocity profile $\omega_b^-(r)$ in Eq. (19).

$$n_b^0(r)=\begin{cases}\hat{n}_b=\text{const}, & a\le r<r_b\\ 0, & r_b<r\le b\ .\end{cases} \tag{18}$$

Substituting Eq. (18) into Eq. (15) gives [Fig. 2(b)]

$$\omega_b^-(r)=\frac{\omega_c}{2}\left\{1-\left[1-\frac{2\hat{\omega}_{pb}^2}{\omega_c^2}\left[1-\frac{a^2}{r^2}\right]\right]^{1/2}\right\} \tag{19}$$

for $a\le r\le r_b$. Here $\hat{\omega}_{pb}^2=4\pi\hat{n}_b e^2/m=\text{const}$. Note that $\omega_b^-(r)$ assumes its maximum value at $r=r_b$. For $a=0$, it follows from Eq. (19) that $\omega_b^-=\text{const}$ and $\partial\omega_b^-/\partial r=0$. For $a\neq 0$, however, there is generally a shear in the angular velocity profile with $\partial\omega_b^-(r)/\partial r\neq 0$.

Finally, an important frequency known as the *vortex* frequency ω_{bv}, enters the subsequent stability analysis. Here, ω_{bv} is defined by

$$\omega_{bv}(r)\equiv\omega_b^+(r)-\omega_b^-(r)=\pm[2\omega_b^{\pm}(r)-\omega_c]\ . \tag{20}$$

From Eq. (14), we find that

$$(\omega_b^+-\omega_b^-)^2=\omega_c^2-\frac{4}{r^2}\int_a^r dr'\,r'\omega_{pb}^2(r')\ . \tag{21}$$

Moreover, $\omega_{pb}^2(r)$ can be expressed directly in terms of $(\omega_b^+-\omega_b^-)^2$ by

$$\omega_{pb}^2(r)=-\frac{1}{4r}\frac{\partial}{\partial r}[r^2(\omega_b^+-\omega_b^-)^2]\ . \tag{22}$$

III. ELECTROSTATIC EIGENVALUE EQUATION FOR NONRELATIVISTIC FLOW IN A CYLINDRICAL DIODE

In this section we derive the eigenvalue equation for small-amplitude electrostatic perturbations about the general class of laminar cold-fluid equilibria described in Sec. II. Assuming $\delta\vec{B}(\vec{x},t)\simeq 0$ and

$$\vec{E}(\vec{x},t)=-\vec{\nabla}\phi(\vec{x},t)\ , \tag{23}$$

each quantity of physical interest is expressed as its equilibrium value plus a perturbation. That is,

$$\begin{aligned}&n_b(\vec{x},t)=n_b^0(r)+\delta n_b(\vec{x},t)\ ,\\ &\vec{V}_b(\vec{x},t)=V_{\theta b}^0(r)\hat{e}_\theta+\delta\vec{V}_b(\vec{x},t)\ ,\\ &\vec{E}(\vec{x},t)=E_r^0(r)\hat{e}_r-\vec{\nabla}\delta\phi(\vec{x},t)\ ,\\ &\vec{B}(\vec{x},t)=B_0\hat{e}_z\ ,\end{aligned} \tag{24}$$

where $\hat{e}_r$, $\hat{e}_\theta$, and $\hat{e}_z$ are unit vectors in the r, θ, and z directions, respectively. For small-amplitude perturbations, the evolution of $\delta n_b(\vec{x},t)$ $\delta\vec{V}_b(\vec{x},t)$, and $\delta\phi(\vec{x},t)$ is determined from the macroscopic cold-fluid-Poisson equations

$$0=\frac{\partial}{\partial t}\delta n_b(\vec{x},t)+\vec{\nabla}\cdot[n_b^0(r)\delta\vec{V}_b(\vec{x},t)+\delta n_b(\vec{x},t)V_{\theta b}^0(r)\hat{e}_\theta]\ , \tag{25}$$

$$\begin{aligned}&\frac{\partial}{\partial t}\delta\vec{V}_b(\vec{x},t)+V_{\theta b}^0(r)\hat{e}_\theta\cdot\vec{\nabla}\delta\vec{V}_b(\vec{x},t)\\ &\quad+\delta\vec{V}_b(\vec{x},t)\cdot\vec{\nabla}[V_{\theta b}^0(r)\hat{e}_\theta]\\ &\quad=\frac{-e}{m}\left[-\vec{\nabla}\delta\phi(\vec{x},t)+\frac{\delta\vec{V}_b(\vec{x},t)\times B_0\hat{e}_z}{c}\right],\end{aligned} \tag{26}$$

$$\vec{\nabla}^2\delta\phi(\vec{x},t)=4\pi e\,\delta n_b(\vec{x},t)\ . \tag{27}$$

To determine the stability properties for perturbations about equilibrium, a normal-mode approach is adopted. It is assumed that the time variation of perturbed quantities is of the form $\exp(-i\omega t)$, where the complex oscillation frequency ω is determined consistently from Eqs. (25)–(27). If $\text{Im}\omega>0$, then the perturbations grow and the equilibrium configuration is *unstable*. In analyzing Eqs. (25)–(27), the perturbations are assumed to be spatially periodic in the z direction. The θ and z dependences of all perturbed quantities are Fourier decomposed according to

$$\delta\psi(r,\theta,z,t)=\sum_{l=-\infty}^{\infty}\sum_{k_z=-\infty}^{\infty}\delta\psi^l(r,k_z)\exp[i(l\theta+k_z z-\omega t)]\ . \tag{28}$$

Substituting Eq. (28) into Eqs. (25)–(27), it can be shown that the Fourier amplitudes $\delta n_b^l(r,k_z)$, $\delta V_{rb}^l(r,k_z)$, etc., satisfy

$$-i(\omega-l\omega_b^-)\delta n_b^l+\frac{1}{r}\frac{\partial}{\partial r}(rn_b^0\delta V_{rb}^l)+\frac{iln_b^0\delta V_{\theta b}^l}{r}+ik_z n_b^0\delta V_{zb}^l=0\ , \tag{29}$$

$$-i(\omega-l\omega_b^-)\delta V_{rb}^l-(-\omega_c+2\omega_b^-)\delta V_{\theta b}^l=\frac{e}{m}\frac{\partial}{\partial r}\delta\phi^l\ , \tag{30}$$

$$-i(\omega-l\omega_b^-)\delta V_{\theta b}^l+\left[-\omega_c+\frac{1}{r}\frac{\partial}{\partial r}(r^2\omega_b^-)\right]\delta V_{rb}^l=\frac{e}{m}\frac{il\,\delta\phi^l}{r}\ , \tag{31}$$

$$-i(\omega-l\omega_b^-)\delta V_{zb}^l=\frac{e}{m}ik_z\,\delta\phi^l\ , \tag{32}$$

$$\frac{1}{r}\frac{\partial}{\partial r}r\frac{\partial}{\partial r}\delta\phi^l-\frac{l^2}{r^2}\delta\phi^l-k_z^2\,\delta\phi^l=4\pi e\,\delta n_b^l\ , \tag{33}$$

where $-e$ is the electron charge, $\omega_c=eB_0/mc$ is the cyclotron frequency, and a slow-rotational equilibrium with $\omega_b(r)=\omega_b^-(r)=V_{\theta b}^0(r)/r$ is assumed in Eqs. (29)–(33). The equilibrium angular velocity $\omega_b^-(r)$ in Eqs. (29)–(33) is related to the equilibrium density profile $n_b^0(r)$ by Eq. (15). The perturbations in density and mean fluid velocities in Eqs. (29)–(32) can be eliminated in favor of $\delta\phi^l(r,k_z)$. Poisson's equation for the perturbed electrostatic potential can then be expressed in the form[14]

$$\frac{1}{r}\frac{\partial}{\partial r}\left[r\left[1-\frac{\omega_{pb}^2}{\nu_b^2}\right]\frac{\partial}{\partial r}\delta\phi^l\right]-\frac{l^2}{r^2}\left[1-\frac{\omega_{pb}^2}{\nu_b^2}\right]\delta\phi^l - k_z^2\left[1-\frac{\omega_{pb}^2}{(\omega-l\omega_b^-)^2}\right]\delta\phi^l = -\frac{l\,\delta\phi^l}{r}\frac{1}{(\omega-l\omega_b^-)}\frac{\partial}{\partial r}\left[\frac{\omega_{pb}^2}{\nu_b^2}(2\omega_b^- -\omega_c)\right], \quad (34)$$

where $\omega_{pb}^2(r)=4\pi n_b^0(r)e^2/m$, and $\nu_b^2(r)$ is defined by

$$\nu_b^2(r)=(\omega-l\omega_b^-)^2-(2\omega_b^- -\omega_c)\left[\frac{1}{r}\frac{\partial}{\partial r}(r^2\omega_b^-)-\omega_c\right]. \quad (35)$$

Equation (34) is valid for arbitrary $\omega_{pb}^2(r)$ and $\omega_b^-(r)$ consistent with Eq. (15). Operationally the procedure is to solve Eq. (34) for $\delta\phi^l(r,k_z)$ and ω as an eigenvalue problem. The solution to Eq. (34) is accessible analytically for certain simple density profiles.

Making use of the definition of $\omega_b^-(r)$ in Eq. (15), the quantity $\nu_b^2(r)$ defined in Eq. (35) can be expressed in the equivalent form

$$\nu_b^2(r)=(\omega-l\omega_b^-)^2-\left[\omega_c^2-\omega_{pb}^2(r)-\frac{2}{r^2}\int_a^r dr'\,r'\omega_{pb}^2(r')\right]. \quad (36)$$

It should be emphasized that the $\omega_{pb}^2(r)$ contributions in Eq. (36) arise from equilibrium space-charge effects associated with $E_r^0(r)\neq 0$. It should also be noted that for a *thin* annulus of electrons (large-aspect-ratio diode) the final term in Eq. (36) is typically small in comparison with $\omega_{pb}^2(r)$. Defining

$$\omega_E(r)\equiv -\frac{cE_r^0(r)}{B_0 r}=\frac{1}{r^2\omega_c}\int_a^r dr'\,r'\omega_{pb}^2(r'), \quad (37)$$

the quantity $\nu_b^2(r)$ in Eq. (36) can also be expressed *exactly* as

$$\nu_b^2(r)=(\omega-l\omega_b^-)^2-[\omega_c^2-\omega_{pb}^2(r)-2\omega_c\omega_E(r)]. \quad (38)$$

Thus far, the electrostatic eigenvalue equation (34) is completely general. We now simplify Eq. (34) for the case of a cylindrical diode with moderately large aspect ratio ($R_0\gg d$ in Fig. 1). In particular, it is assumed that

$$\omega_E(r)=\frac{1}{\omega_c r^2}\int_a^r dr'\,r'\omega_{pb}^2(r')\ll\omega_c \quad (39)$$

over the radial extent of the electron plasma. Note that Eq. (39) does *not* require that the electron density be low with $\omega_{pb}^2(r)\ll\omega_c^2$. Rather, evaluating Eq. (39) at $r=b$, the inequality in Eq. (39) is satisfied whenever

$$\frac{\hat{\omega}_{pb}^2}{\omega_c^2}\frac{\Delta}{R_0}\ll 1, \quad (40)$$

where $\hat{\omega}_{pb}^2=4\pi\hat{n}_b e^2/m$, $\hat{n}_b$ is the characteristic (average) electron density, and $\Delta(\ll R_0)$ is the characteristic radial width of the electron density profile. Making use of Eq. (39), it follows from Eqs. (15) and (38) that $\omega_b^-(r)$ and $\nu_b^2(r)$ can be approximated by

$$\omega_b^-(r)=\omega_E(r), \quad (41)$$

and

$$\nu_b^2(r)=[\omega-l\omega_E(r)]^2-[\omega_c^2-\omega_{pb}^2(r)]. \quad (42)$$

Moreover, within the context of Eqs. (39), (41), and (42), the electrostatic eigenvalue equation (34) can be approximated by

$$\frac{1}{r}\frac{\partial}{\partial r}\left[r\left[1-\frac{\omega_{pb}^2}{(\omega-l\omega_E)^2-(\omega_c^2-\omega_{pb}^2)}\right]\frac{\partial}{\partial r}\delta\phi^l\right]-\frac{l^2}{r^2}\left[1-\frac{\omega_{pb}^2}{(\omega-l\omega_E)^2-(\omega_c^2-\omega_{pb}^2)}\right]\delta\phi^l-k_z^2\left[1-\frac{\omega_{pb}^2}{(\omega-l\omega_E)^2}\right]\delta\phi^l = \frac{l\delta\phi^l}{r}\frac{\omega_c}{(\omega-l\omega_E)}\frac{\partial}{\partial r}\left[\frac{\omega_{pb}^2}{(\omega-l\omega_E)^2-(\omega_c^2-\omega_{pb}^2)}\right], \quad (43)$$

where $\omega_{pb}^2(r)=4\pi r_b^0(r)e^2/m$, and $\omega_E(r)$ is defined in Eq. (37).

IV. STABILITY THEOREM FOR LOW-FREQUENCY FLUTE PERTURBATIONS

A. Sufficient condition for stability

The electrostatic eigenvalue equation (43) can be solved numerically for the eigenfunction $\delta\phi^l$ and the eigenfrequency ω for a broad range of electron density profiles $n_b^0(r)$, and specific numerical examples are presented in Sec. VI. In this section, we make use of Eq. (43) to determine a sufficient condition for $n_b^0(r)$ to be stable for low-frequency flute perturbations with

$$k_z=0. \quad (44)$$

In particular, it is assumed that the electron density is below the condition for Brillouin flow

$$\omega_{pb}^2(r)<\omega_c^2. \quad (45)$$

[Note that $\omega_{pb}^2(r)\ll\omega_c^2$ is not required for proof of the stability theorem later in this section.] The eigenvalue equation (43) generally supports both high-frequency and low-frequency solutions. For present purposes, we examined Eq. (43) for low-frequency perturbations satisfying

$$|\omega-l\omega_E(r)|^2\ll\omega_c^2-\omega_{pb}^2(r). \quad (46)$$

Making use of Eqs. (44) and (46), the eigenvalue equation (43) can be approximated by

$$\frac{1}{r}\frac{\partial}{\partial r}\left[r\left[1+\frac{\omega_{pb}^2(r)}{\omega_c^2-\omega_{pb}^2(r)}\right]\frac{\partial}{\partial r}\delta\phi^l\right]-\frac{l^2}{r^2}\left[1+\frac{\omega_{pb}^2(r)}{\omega_c^2-\omega_{pb}^2(r)}\right]\delta\phi^l=-\frac{l\delta\phi^l}{r}\frac{\omega_c}{\omega-l\omega_E(r)}\frac{\omega_c^2}{[\omega_c^2-\omega_{pb}^2(r)]^2}\frac{\partial}{\partial r}\omega_{pb}^2(r)\ . \tag{47}$$

In Eq. (47), note that

$$\epsilon_\perp(r)=1+\frac{\omega_{pb}^2(r)}{\omega_c^2-\omega_{pb}^2(r)} \tag{48}$$

is the effective perpendicular dielectric function, and

$$\omega=\omega_r+i\gamma \tag{49}$$

is the complex eigenfrequency, with $\gamma=\mathrm{Im}\omega>0$ corresponding to instability. Moreover, the boundary conditions used in solving Eq. (47) are

$$\delta\phi^l(r=a)=0=\delta\phi^l(r=b)\ , \tag{50}$$

which assures that the tangential electric field $\delta E_\theta^l=-il\delta\phi^l/r$ is equal to zero at the perfect conducting cathode ($r=a$) and anode ($r=b$).

The main objective here is to make use of the approximate eigenvalue equation (47) to extend to higher density the classical stability theorem first derived by Briggs *et al.*[17] for the case $\omega_{pb}^2(r)\ll\omega_c^2$. To determine a sufficient condition for stability, we multiply Eq. (47) by $r\delta\phi^{l*}$ and integrate from $r=a$ to $r=b$. This gives

$$0=D(\omega)=\int_a^b dr\,r\left[\left[\left|\frac{\partial}{\partial r}\delta\phi^l\right|^2+\frac{l^2}{r^2}|\delta\phi^l|^2\right]\left[1+\frac{\omega_{pb}^2(r)}{\omega_c^2-\omega_{pb}^2(r)}\right]-\frac{l|\delta\phi^l|^2}{r}\frac{\omega_c}{\omega-l\omega_E(r)}\frac{\omega_c^2}{[\omega_c^2-\omega_{pb}^2(r)]^2}\frac{\partial}{\partial r}\omega_{pb}^2(r)\right]\ . \tag{51}$$

Expressing

$$\frac{1}{\omega_r-l\omega_E+i\gamma}=\frac{(\omega_r-l\omega_E)-i\gamma}{(\omega_r-l\omega_E)^2+\gamma^2}\ , \tag{52}$$

we equate the real and imaginary parts of Eq. (51) separately to zero. The condition $D_r=\mathrm{Re}D(\omega)=0$ gives

$$0=\mathrm{Re}D(\omega)=\int_a^b dr\,r\left[\left[\left|\frac{\partial}{\partial r}\delta\phi^l\right|^2+\frac{l^2}{r^2}|\delta\phi^l|^2\right]\left[1+\frac{\omega_{pb}^2}{\omega_c^2-\omega_{pb}^2(r)}\right]-\frac{l|\delta\phi^l|^2}{r}\frac{\omega_c[\omega_r-l\omega_E(r)]}{[\omega_r-l\omega_E(r)]^2+\gamma^2}\frac{\omega_c^2}{[\omega_c^2-\omega_{pb}^2(r)]^2}\frac{\partial}{\partial r}\omega_{pb}^2(r)\right]\ , \tag{53}$$

whereas $D_i=\mathrm{Im}D(\omega)=0$ gives

$$0=\mathrm{Im}D(\omega)=l\gamma\int_a^b dr\,|\delta\phi^l|^2\frac{\omega_c}{[\omega_r-l\omega_E(r)]^2+\gamma^2}\frac{\omega_c^2}{[\omega_c^2-\omega_{pb}^2(r)]^2}\frac{\partial}{\partial r}\omega_{pb}^2(r)\ . \tag{54}$$

A sufficient condition for electrostatic stability follows from Eq. (54). Let us assume that the density profile is monotonic decreasing with

$$\frac{\partial}{\partial r}\omega_{pb}^2(r)\le 0 \tag{55}$$

over the interval $a\le r\le b$, *and* that the system is *unstable* with $\gamma=\mathrm{Im}\omega>0$. From Eq. (55), it follows that the integral in Eq. (54) is nonzero. Therefore, our assumption of instability ($\gamma>0$) is *incorrect* for monotonic decreasing density profiles, and it neccessarily follows that the system is *stable* whenever Eq. (55) is satisfied over the interval $a\le r\le b$. That is, Eq. (55) corresponds to a *sufficient condition for stability.* Expressed another way, for instability to exist it is *necessary* that $\partial\omega_{pb}^2/\partial r$ change sign in the interval $a\le r\le b$, or equivalently that

$$\frac{1}{r}\frac{\partial}{\partial r}[r^2\omega_E(r)]$$

change sign in the interval $a\le r\le b$, corresponding to a shear in the angular velocity profile.

We emphasize the powerful nature of the stability theorem in Eq. (55). For low-frequency flute perturbations satisfying Eqs. (44)–(46), all monotonic decreasing density profiles with $\partial\omega_{pb}^2/\partial r\le 0$ are electrostatically stable. This stability condition has been derived without specifying the functional form of $n_b^0(r)$ or solving explicitly for the eigenfunction $\delta\phi^l(r)$. Equation (55) represents an important extension to higher density of the stability theorem first derived by Briggs *et al.*[17] for the case $\omega_{pb}^2(r)\ll\omega_c^2$, i.e., $\epsilon_\perp(r)=1$.

The stability theorem derived in this section represents a *direct* calculation of the sufficient condition [Eq. (55)] for the equilibrium density profile $n_b^0(r)$ to be stable for low-frequency flute perturbations. The calculation is *direct* in the sense that it makes explicit use of the eigenvalue equation (47). In a recent calculation,[25] we give an *indirect* proof of this stability condition, based on *global*

conservation constraints satisfied by the fully nonlinear macroscopic fluid equations in the guiding-center approximation with $\omega_{pb}^2 \ll \omega_c^2$ and $m \to 0$.

Finally, for $\omega_{pb}^2 \ll \omega_c^2$, this important stability theorem has its analog in relativistic planar geometry[20,24] and can be extended to include the (stabilizing) influence of finite k_z (Ref. 21) or magnetic shear.[20] We reiterate that the present analysis is restricted to low-frequency perturbations [Eq. (46)] and large aspect ratio [Eq. (39]. Therefore, the possibility of high-frequency (large l) instability discussed by Buneman *et al.*[16] for planar geometry is necessarily excluded, as are the important cylindrical effects associated with finite aspect ratio which are contained in the exact eigenvalue equation (34) analyzed in Sec. VI.

B. Growth rate for weak resonant instability

From Eq. (51), it is straightforward to derive a formal expression for the growth rate γ in circumstances where the instability growth rate $\gamma = \mathrm{Im}\omega$ is weak with

$$|\gamma| \ll |\omega_r| \ . \tag{56}$$

In particular, for small γ, we express

$$D(\omega_r + i\gamma) = D_r(\omega_r) + i\left[D_i(\omega_r) + \gamma \frac{\partial D_r}{\partial \omega_r}\right] + \cdots \ , \tag{57}$$

and make use of

$$\lim_{\gamma \to 0_+} \frac{1}{\omega_r - l\omega_E + i\gamma} = \frac{\mathrm{P}}{\omega_r - l\omega_E} - i\pi\delta(\omega_r - l\omega_E(r)) \ , \tag{58}$$

where P denotes Cauchy principal value. Substituting Eqs. (57) and (58) into Eq. (51) and setting real and imaginary parts equal to zero gives

$$0 = D_r(\omega_r)\int_a^b dr\, r\left[\left|\left|\frac{\partial}{\partial r}\delta\phi^l\right|^2 + \frac{l^2}{r^2}|\delta\phi^l|^2\right]\left[1 + \frac{\omega_{pb}^2(r)}{\omega_c^2 - \omega_{pb}^2(r)}\right] - \frac{l|\delta\phi^l|^2}{r}\mathrm{P}\frac{\omega_c}{\omega_r - l\omega_E(r)}\frac{\omega_c^2}{[\omega_c^2 - \omega_{pb}^2(r)]^2}\frac{\partial}{\partial r}\omega_{pb}^2(r)\right] , \tag{59}$$

and

$$\gamma = \frac{-D_i(\omega_r)}{\partial D_r/\partial\omega_r} = -\pi l\int_a^b dr\,|\delta\phi^l|^2 \frac{\omega_c^3\delta(\omega_r - l\omega_E(r))}{[\omega_c^2 - \omega_{pb}^2(r)]^2}\frac{\partial}{\partial r}\omega_{pb}^2(r) \times \left[\int_a^b dr\,|\delta\phi^l|^2 \mathrm{P}\frac{l\omega_c}{[\omega_r - l\omega_E(r)]^2}\frac{\omega_c^2}{[\omega_c^2 - \omega_{pb}^2(r)]^2}\frac{\partial}{\partial r}\omega_{pb}^2(r)\right]^{-1} . \tag{60}$$

Equation (59) determines the real frequency ω_r (assuming that $\delta\phi^l$ is known), whereas the growth rate γ is given by Eq. (60).

In circumstances where $\partial D_r/\partial\omega_r < 0$, it follows from Eq. (60) that resonant instability exists whenever

$$\left.\frac{\partial\omega_{pb}^2}{\partial r}\right|_{r=r_s} > 0 \ , \tag{61}$$

where the resonant radius r_s satisfies

$$\omega_r - l\omega_E(r_s) = 0 \ . \tag{62}$$

Density profiles $n_b^0(r)$ with a *gentle bump* (Fig. 3) are prime candidates for such a weak *resonant* instability. A specific example is discussed in Sec. V.

V. ANALYTIC SOLUTIONS TO ELECTROSTATIC EIGENVALUE EQUATION

A. Stable surface waves

In this section we make use of the approximate eigenvalue (47) to investigate stability properties for low-frequency flute perturbations with $|\omega - l\omega_E|^2 \ll \omega_c^2 - \omega_{pb}^2(r)$ and $\omega_{pb}^2(r) < \omega_c^2$ [Eqs. (45) and (46)]. As a specific example that is analytically tractable, consider the rectangular density profile (Fig. 2) specified by

$$n_b^0(r) = \begin{cases} \hat{n}_b = \text{const}, & a \le r < r_b \\ 0, & r_b < r \le b \ . \end{cases} \tag{63}$$

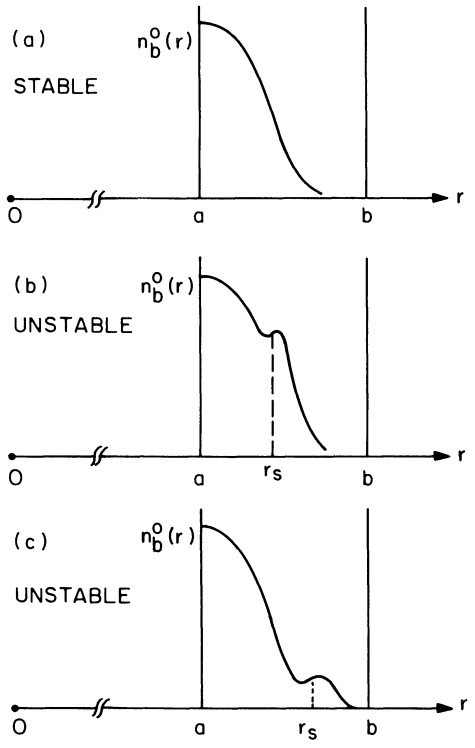

FIG. 3. Class of equilibrium density profiles $n_b^0(r)$ that are (a) stable [Eq. (55)], (b) unstable [Eq. (61)], and (c) unstable [Eq. (61)], for low-frequency flute perturbations satisfying Eqs. (44)–(46).

From Eqs. (37) and (63), $\omega_E(r)=-cE_r^0(r)/rB_0$ can be expressed as (for $a\le r<r_b$)

$$\omega_E(r)=\frac{\hat{\omega}_{pb}^2}{2\omega_c}\left[\frac{r^2-a^2}{a^2}\right], \tag{64}$$

where $\hat{\omega}_{pb}^2=4\pi\hat{n}_b e^2/m=$const. Because $\omega_{pb}^2(r)=\hat{\omega}_{pb}^2$ =const for $a\le r<r_b$ (region I), the eigenvalue equation (47) reduces to

$$\frac{1}{r}\frac{\partial}{\partial r}r\frac{\partial}{\partial r}\delta\phi_{\rm I}^l-\frac{l^2}{r^2}\delta\phi_{\rm I}^l=0,\quad a\le r<r_b \tag{65}$$

within the electron annulus. Moreover, because $\omega_{pb}^2(r)=0$ for $r_b<r\le b$ (region II), the eigenvalue equation (47) can be expressed as

$$\frac{1}{r}\frac{\partial}{\partial r}r\frac{\partial}{\partial r}\delta\phi_{\rm II}^l-\frac{l^2}{r^2}\delta\Phi_{\rm II}^l=0,\quad r_b<r\le b \tag{66}$$

in the vacuum region between the anode and surface of the electron annulus. The solutions to Eqs. (65) and (66) that satisfy $\delta\phi_{\rm I}^l(r=a)=0=\delta\phi_{\rm II}^l(r=b)$ and are continuous at $r=r_b$ are given by

$$\delta\phi_{\rm I}^l(r)=A\left[\left[\frac{r}{a}\right]^l-\left[\frac{a}{r}\right]^l\right],\quad a\le r<r_b \tag{67}$$

and

$$\delta\phi_{\rm II}^l(r)=A\left[\left[\frac{r}{b}\right]^l-\left[\frac{b}{r}\right]^l\right]\left[\left[\frac{r_b}{a}\right]^l-\left[\frac{a}{r_b}\right]^l\right]\left[\left[\frac{r_b}{b}\right]^l-\left[\frac{b}{r_b}\right]^l\right]^{-1},\quad r_b<r\le b\ . \tag{68}$$

The remaining boundary condition on $(\partial/\partial r)\delta\phi^l$ at $r=r_b$ is obtained by integrating the eigenvalue equation (47) across the surface of the plasma at $r=r_b$. Multiplying Eq. (47) by r and integrating from $r_b(1-\epsilon)$ to $r_b(1+\epsilon)$, with $\epsilon\to 0_+$, gives

$$\left[r\frac{\partial}{\partial r}\delta\phi_{\rm II}^l\right]_{r=r_b}-\left[1+\frac{\hat{\omega}_{pb}^2}{(\omega_c^2-\omega_{pb}^2)}\right]\left[r\frac{\partial}{\partial r}\delta\phi_{\rm I}^l\right]_{r=r_b}=\frac{l\delta\phi^l(r=r_b)\omega_c}{[\omega-l\omega_E(r_b)]}\frac{\hat{\omega}_{pb}^2}{(\omega_c^2-\hat{\omega}_{pb}^2)}, \tag{69}$$

where $\hat{\omega}_{pb}^2=4\pi\hat{n}_b e^2/m$, and

$$\omega_E(r_b)=\frac{\hat{\omega}_{pb}^2}{2\omega_c}\left[\frac{r_b^2-a^2}{a^2}\right]. \tag{70}$$

Equation (69) relates the discontinuity in perturbed radial electric field to the perturbed surface charge density at $r=r_b$. It is useful to define

$$\hat{\epsilon}_\perp=1+\frac{\hat{\omega}_{pb}^2}{(\omega_c^2-\hat{\omega}_{pb}^2)}=\frac{\omega_c^2}{(\omega_c^2-\hat{\omega}_{pb}^2)},$$
$$\hat{\Omega}_D=\frac{\hat{\omega}_{pb}^2}{2\omega_c}, \tag{71}$$

and

$$\frac{1}{g_l}=\left[\left[\frac{r_b}{b}\right]^l+\left[\frac{b}{r_b}\right]^l\right]\left[\left[\frac{r_b}{b}\right]^l-\left[\frac{b}{r_b}\right]^l\right]^{-1}-\hat{\epsilon}_\perp\left[\left[\frac{r_b}{a}\right]^l+\left[\frac{a}{r_b}\right]^l\right]\left[\left[\frac{r_b}{a}\right]^l-\left[\frac{a}{r_b}\right]^l\right]^{-1}, \tag{72}$$

where g_l is an effective geometric factor. Substituting Eqs. (67) and (68) into Eq. (69) then gives

$$\frac{1}{g_l}=\frac{2\hat{\Omega}_D\hat{\epsilon}_\perp}{\omega-l\omega_E(r_b)}, \tag{73}$$

or equivalently,

$$\omega-l\omega_E(r_b)=(2g_l\hat{\epsilon}_\perp)\hat{\Omega}_D\ . \tag{74}$$

Note that Eq. (69) has played the role of an effective dispersion relation that determines the eigenfrequency ω. From Eq. (74), for the rectangular density profile in Eq. (63) and Fig. 2, the system supports only stable oscillations (Im$\omega=0$). On the other hand, a completely analogous analysis of the eigenvalue equation (47) can be carried out for the hollow density profile illustrated in Fig. 4, where the inner surface of the electron annulus is separated from the cathode. In this case, there are charge perturbations on the inner surface ($r=r_b^-$) as well as the outer surface ($r=r_b^+$) of the annulus, and the interaction leads to the familiar *diocotron instability*[15–18] modified to include plasma dielectric effects with $\hat{\epsilon}_\perp-1>0$.

To conclude this section, we simplify the expression for the geometric factor g_l in Eq. (72) for a moderate-aspect-ratio diode with

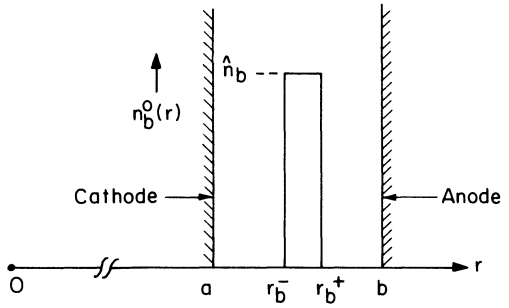

FIG. 4. Hollow electron density profile that exhibits strong diocotron instability (see Ref. 10).

$$a \gg d = (b-a) , \tag{75}$$

and for (low) harmonic numbers l satisfying

$$\frac{ld}{a} \ll 1 . \tag{76}$$

To leading order, Eq. (72) gives the approximate expression for g_l

$$\frac{1}{g_l} = \left[1 - \frac{a+d}{l[d-(r_b-a)]} \right] - \hat{\epsilon}_\perp \left[1 + \frac{a}{l(r_b-a)} \right] , \tag{77}$$

where $l(r_b-a)/a \ll 1$ is assumed, and $d=b-a$ is the anode-cathode spacing. We denote (Fig. 5) the thickness of the annulus by Δ_a and the width of the vacuum region by Δ_v where

$$\begin{aligned} \Delta_a &= r_b - a , \\ \Delta_v &= d-(r_b-a) = b - r_b . \end{aligned} \tag{78}$$

For $l\Delta_a/a \ll 1$ and $l\Delta_v/a \ll 1$, Eq. (77) can be approximated by

$$g_l = - \frac{l\Delta_v/b}{1+\hat{\epsilon}_\perp(\Delta_v a/\Delta_a b)} . \tag{79}$$

For a thin annulus, it follows from Eq. (64) that $\omega_E(r)$ can be approximated by

$$\omega_E(r) = 2\hat{\Omega}_D \left[\frac{r-a}{a} \right] , \tag{80}$$

and $\omega_E(r_b)$ by

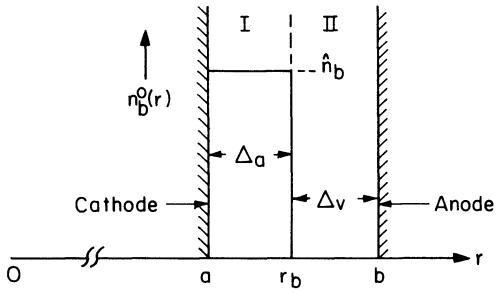

FIG. 5. Rectangular density profile $n_b^0(r)$ assumed in stability analysis in Sec. V A. A large-aspect-ratio diode with $a \gg \Delta_a$, Δ_v is assumed.

$$\omega_E(r_b) = 2\frac{\Delta_a}{a}\hat{\Omega}_D , \tag{81}$$

where $\hat{\Omega}_D = \hat{\omega}_{pb}^2/2\omega_c$. For $b \simeq a$, we substitute the approximate expression (79) for g_l into Eq. (74). This gives

$$\omega - l\omega_E(r_b) = - \frac{\hat{\epsilon}_\perp}{1+\hat{\epsilon}_\perp \Delta_v/\Delta_a} 2l\frac{\Delta_v}{a}\hat{\Omega}_D , \tag{82}$$

where $\omega_E(r_b)$ is defined in Eq. (81). Since $ld/a \ll 1$ has been assumed in Eq. (82), it follows that the low-frequency assumption, $|\omega - l\omega_E|^2 \ll \omega_c^2 - \hat{\omega}_{pb}^2$ in Eq. (46), is readily satisfied for moderate values of $\hat{\omega}_{pb}^2/\omega_c^2$.

B. Resonant diocotron instability

We now consider circumstances where the main density region ($a \le r < r_b$) is seeded with a low-density component of circulating electrons (Fig. 6). In the low-density regime, it is well known that such a density profile can lead to a resonant version[17] of the classical diocotron instability.[14–18] In the region $a \le r < r_b$, $\omega_E(r) = -cE_r^0(r)/B_0$ is still given approximately by Eq. (80) because $E_r^0(r)$ is determined primarily by the main density component ($\hat{n}_b$) in Fig. 6. That is, $\omega_E(r)$ can be approximated by

$$\omega_E(r) = 2\hat{\Omega}_D \left[\frac{r-a}{a} \right] , \quad a \le r < r_b \tag{83}$$

in the region of the low-density bump in Fig. 6. Moreover, the analytic results in Sec. VI A represent excellent approximations for the eigenfunctions in regions I and II [Eqs. (67) and (68)], and for the real oscillation frequency $\omega_r = \mathrm{Re}\omega$ [Eq. (82)] in circumstances where the bump density is much less than $\hat{n}_b$. That is, $\omega_r = \mathrm{Re}\omega$ is given approximately by

$$\omega_r - l\omega_E(r_b) = - \frac{\hat{\epsilon}_\perp}{1+\hat{\epsilon}_\perp \Delta_v/\Delta_a} 2l\frac{\Delta_v}{a}\hat{\Omega}_D \tag{84}$$

for a large-aspect-ratio diode with $ld/a \ll 1$.

In Sec. IV B, we derived a formal expression [Eq. (60)] for the growth rate $\gamma = \mathrm{Im}\omega$ assuming (weak) resonant instability driven by a gentle bump in the density profile $n_b^0(r)$. From Eqs. (61) and (62), the condition for instability is

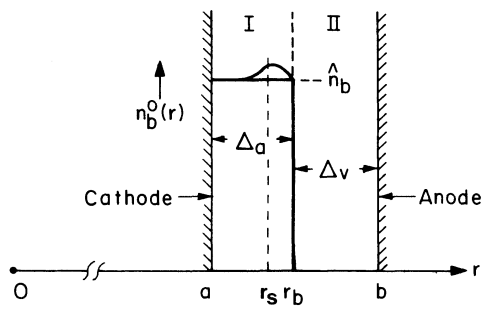

FIG. 6. Density profile $n_b^0(r)$ with density bump that leads to the resonant diocotron instability discussed in Sec. V B.

$$\left.\frac{\partial n_b^0}{\partial r}\right|_{r=r_s} > 0 , \tag{85}$$

where r_s solves the resonance condition

$$\omega_r - l\omega_E(r_s) = 0 . \tag{86}$$

Substituting Eqs. (83) and (84) into Eq. (86), and solving for r_s gives

$$r_s = r_b \left[1 - \frac{\hat{\epsilon}_\perp}{1+\hat{\epsilon}_\perp \Delta_v/\Delta_a} \frac{\Delta_v}{r_b} \right] , \tag{87}$$

which determines the resonant radius r_s that satisfies Eq. (86). For example, if $\hat{\epsilon}_\perp = 1.5$ and $\Delta_v/\Delta_a = \frac{2}{3}$, then $r_s - r_b = -0.5\Delta_a$ follows from Eq. (87).

The expression for growth rate γ is given in Eq. (60). Assuming that r_s satisfies $a < r_s < r_b$ [Eq. (87) and Fig. 6], then $D_i(\omega_r) = \mathrm{Im}D(\omega)$ is given by [Eq. (60)].

$$D_i(\omega_r) = \frac{\pi a \hat{\epsilon}_\perp^2}{(2\omega_c \hat{\Omega}_D)} \left| \delta\phi_{\mathrm{I}}^l \right|^2_{r=r_s} \left. \frac{\partial}{\partial r} \omega_{pb}^2(r) \right|_{r=r_s} , \tag{88}$$

where use has been made of $\partial\omega_E/\partial r \,|_{r=r_s} = 2\hat{\Omega}_d/a$ [Eq. (12)]. In Eq. (88), $\delta\phi_{\mathrm{I}}^l(r)$ is approximated by Eq. (67), i.e., by the eigenfunction in region I in the absence of density bump. Similarly, $\partial D_r/\partial\omega_r$ is given by [Eq. (60)]

$$\frac{\partial D_r}{\partial \omega_r} = - \left| \delta\phi_{\mathrm{I}}^l \right|^2_{r=r_b} \frac{2l\hat{\Omega}_D \hat{\epsilon}_\perp}{[\omega_r - l\omega_E(r_b)]^2} , \tag{89}$$

where $\delta\phi_{\mathrm{I}}^l(r)$ is approximated by (67), $\hat{\epsilon}_\perp$ is defined in Eq. (71), and $\hat{\Omega}_D = \hat{\omega}_{pb}^2/2\omega_c$. Note from Eq. (60), Eq. (89), and Fig. 6 that the main contribution to $\partial D_r/\partial\omega_r$ comes from the density discontinuity at the surface ($r = r_b$) of the electron annulus. Combining Eqs. (88) and (89), the growth rate $\gamma = -D_i/(\partial D_r/\partial\omega_r)$ is

$$\gamma = \frac{\pi\hat{\epsilon}_\perp}{4l} \frac{[\omega_r - l\omega_E(r_b)]^2}{\hat{\Omega}_D^2} \frac{\left| \delta\phi_{\mathrm{I}}^l \right|^2_{r=r_s}}{\left| \delta\phi_{\mathrm{I}}^l \right|^2_{r=r_b}} \frac{a}{\omega_c} \left. \frac{\partial}{\partial r} \omega_{pb}^2 \right|_{r=r_s} , \tag{90}$$

where $\omega_r - l\omega_E(r_b)$ is given in Eq. (84). From Eqs. (67) and (68),

$$\frac{\left| \delta\phi_{\mathrm{I}}^l \right|^2_{r=r_s}}{\left| \delta\phi_{\mathrm{I}}^l \right|^2_{r=r_b}} = \left[\left[\left(\frac{r_a}{a} \right)^l - \left(\frac{a}{r_s} \right)^l \right]^2 \left[\left(\frac{r_b}{a} \right)^l - \left(\frac{a}{r_b} \right)^l \right]^{-2} \right] \simeq \left[\frac{r_s - a}{r_b - a} \right]^2 , \tag{91}$$

for a large-aspect-ratio diode with $l(r_s - a)$, $l(r_b - a) \ll a$. Defining $r_b - a = \Delta_a$ (Fig. 6), and making use of $r_s - a = r_b - a - (r_b - r_s) = \Delta_a(1 + \epsilon_\perp \Delta_v/\Delta_a)^{-1}$ [Eq. (87)], the ratio in Eq. (91) can be approximated by

$$\frac{\left| \delta\phi_{\mathrm{I}}^l \right|^2_{r=r_s}}{\left| \delta\phi_{\mathrm{I}}^l \right|^2_{r=r_b}} = \frac{1}{(1+\epsilon_\perp \Delta_v/\Delta_a)^2} . \tag{92}$$

Returning to Eq. (90), we normalize the growth rate γ to $l\omega_E(r_b) = 2l\hat{\Omega}_D\Delta_a/a$, where $\Delta_a = r_b - a$ and $\omega_E(r_b)$ is given in Eq. (81). Making use of Eqs. (82) and (92), the normalized growth rate $\gamma/l\omega_E(r_b)$ in Eq. (90) can be expressed as

$$\frac{\gamma}{l\omega_E(r_b)} = \frac{\pi\hat{\epsilon}_\perp^3 \Delta_a^2 \Delta_v^2}{(\Delta_a + \hat{\epsilon}_\perp \Delta_v)^4} \frac{\Delta_a}{\hat{\omega}_{pb}^2} \left. \frac{\partial}{\partial r} \omega_{pb}^2(r) \right|_{r=r_s} , \tag{93}$$

where $\hat{\omega}_{pb}^2 = 2\omega_c\hat{\Omega}_D = 4\pi\hat{n}_b e^2/m$ is the plasma frequency, squared of the main density component ($\hat{n}_b$) in Fig. 6.

Measured in units of $l\omega_E(r_b)$, the growth rate γ in Eq. (93) can be substantial. The *resonant diocotron instability* discussed in this section may well be one of the most important instabilities characteristic of electron flow in diodes. Although monotonic decreasing profiles with $\partial n_b^0/\partial r \le 0$ are stable [Figs. 3(a) or 5], the introduction of a low-density circulating electron component [Figs. 3(b), 3(c), or 6] can lead to resonant instability.

VI. NUMERICAL SOLUTION TO ELECTROSTATIC EIGENVALUE EQUATION

In this section we make use of the exact electrostatic eigenvalue equation (34) to investigate numerically the stability properties of a variety of equilibrium profiles $n_b^0(r)$.

A. Eigenvalue equation

For nonrelativistic, cold-fluid flow, the *exact* electrostatic eigenvalue equation in cylindrical geometry is given by Eq. (34). It is convenient to introduce the dimensionless radial coordinate

$$R = \frac{r}{a} , \tag{94}$$

where $r = a$ is the location of the cathode (Fig. 1). Moreover, all frequencies are normalized to $\omega_c = eB_0/mc$ with

$$\hat{\omega}_E(r) \equiv \frac{\omega_E(r)}{\omega_c} = \frac{1}{r^2\omega_c^2} \int_a^r dr' \, r' \omega_{pb}^2(r') , \quad \hat{\omega} \equiv \frac{\omega}{\omega_c}$$

$$\hat{\omega}_{pb}^2(r) \equiv \frac{\omega_{pb}^2(r)}{\omega_c^2} = \frac{4\pi n_b^0(r) e^2}{m\omega_c^2} , \tag{95}$$

$$\hat{\omega}_b^-(r) \equiv \frac{\omega_b^-(r)}{\omega_c} = \tfrac{1}{2}\{1 - [1 - 4\hat{\omega}_E(r)]^{1/2}\} .$$

Making use of Eqs. (94) and (95), the eigenvalue equation (34) can be expressed in the equivalent form

$$\frac{1}{R}\frac{\partial}{\partial R}\left[R\left[1-\frac{\hat{\omega}_{pb}^2}{(\hat{\omega}-l\hat{\omega}_b^-)^2-(1-\hat{\omega}_{pb}^2-2\hat{\omega}_E)}\right]\frac{\partial}{\partial R}\delta\phi^l-\frac{l^2}{R^2}\left[1-\frac{\hat{\omega}_{pb}^2}{(\hat{\omega}-l\hat{\omega}_b^-)^2-(1-\hat{\omega}_{pb}^2-2\hat{\omega}_E)}\right]\delta\phi^l\right.$$
$$=\frac{l\delta\phi^l}{R}\frac{1}{(\hat{\omega}-l\hat{\omega}_b^-)}\frac{\partial}{\partial R}\left[\frac{\hat{\omega}_{pb}^2(1-4\hat{\omega}_E)^{1/2}}{(\hat{\omega}-l\hat{\omega}_b^-)^2-(1-\hat{\omega}_{pb}^2-2\hat{\omega}_E)}\right], \quad (96)$$

where $k_z=0$ is assumed, and the dimensionless frequencies $\hat{\omega}$, $\hat{\omega}_{pb}^2(r)$, and $\hat{\omega}_E(r)$ are defined in Eq. (95). The equilibrium boundary condition assumed in Eq. (96) is $E_r^0(r=a)=0$ at the cathode, which corresponds to $\hat{\omega}_E(r=a)=0$. Note also that the eigenvalue equation (96) is exact within the context of the present electrostatic model based on the nonrelativistic cold-fluid-Possion equations. That is, unlike the approximate eigenvalue equations analyzed in Secs. IV and V, there is no *a priori* assumption in Eq. (96) that $\omega_E(r)\ll\omega_c$ [as in Eq. (39)], that the perturbation frequency is low [as in Eq. (46)], or that the diode aspect ratio is large [as in Eq. (75)].

In Secs. VI B and VI C, Eq. (96) is solved numerically for the real oscillation frequency $\omega_r=\mathrm{Re}\omega$, the growth rate $\gamma=\mathrm{Im}\omega$, and the eigenfunction $\delta\phi^l(r)$ subject to the boundary conditions

$$\delta\phi^l=0 \text{ at } r=a \text{ and at } r=b\ . \quad (97)$$

Depending on the choice of equilibrium density profile $n_b^0(r)$, the solutions to Eq. (96) correspond to weakly unstable oscillations (Sec VI B) or to strong instability (Sec. VI C).

B. Weakly unstable oscillations

As a first example of an equilibrium density profile that gives weakly unstable oscillations, consider the rectangular density profile specified by (Fig. 2)

$$n_b^0(r)=\begin{cases}\hat{n}_b=\text{const}, & a\le r<r_b\\ 0, & r_b<r\le b\ .\end{cases} \quad (98)$$

TABLE I. $\mathrm{Re}\omega/\omega_c$ and $\mathrm{Im}\omega/\omega_c$ versus l [Eq. (96)] for $b/a=3$, $r_b/a=2$, and (a) $s=0.5$, and (b) $s=0.2$, for the rectangular density profile in Eq. (98).

l	$\mathrm{Re}\omega/\omega_c$	$\mathrm{Im}\omega/\omega_c$
	(a) $s=\omega_{pb}^2/\omega_c^2=0.5$	
1	0.066	0.59×10^{-2}
2	0.209	1.32×10^{-2}
3	0.417	2.35×10^{-2}
4	0.658	2.44×10^{-2}
5	0.867	0.26×10^{-2}
	(b) $s=\omega_{pb}^2/\omega_c^2=0.2$	
1	0.028	1.65×10^{-4}
2	0.077	2.79×10^{-4}
3	0.143	2.49×10^{-4}
4	0.219	1.76×10^{-4}
5	0.298	1.22×10^{-4}

Equation (96) has been solved numerically for the complex eigenfrequency $\omega=\omega_r+i\gamma$ and eigenfunction $\delta\phi^l(r)$ assuming $r_b/a=2$ and $b/a=3$. Typical results are illustrated in Table I, where $\omega_r=\mathrm{Re}\omega$ and $\gamma=\mathrm{Im}\omega$ are tabulated versus azimuthal mode number $l=1,2,3,4,5$ for the low-frequency branch that solves Eq. (96). The values chosen for the dimensionless self-field parameter $s\equiv4\pi\hat{n}_bmc^2/B_0^2=\omega_{pb}^2/\omega_c^2$ correspond to $s=0.5$ [Table I(a)] and $s=0.2$ [Table I(b)]. Note from Table I(a) and I(b) that the system is *weakly unstable* ($\gamma\ll|\omega_r|$) for the choice of rectangular density profile in Eq. (98). Moreover, the collisionless growth is weakest for low values of electron density (small values of s).

As a second example, we consider the bell-shaped density profile specified by (Fig. 7).

$$n_b^0(r)=\begin{cases}\hat{n}_b\left[1-\dfrac{(r-a)^2}{(r_b-a)^2}\right]^2, & a\le r<r_b\\ 0, & r_b<r\le b\ .\end{cases} \quad (99)$$

Note from Eq. (99) that $n_b^0(r)$ decreases monotonically from $\hat{n}_b$ at $r=a$ to zero at $r=r_b$. The complex eigenfrequency $\omega=\omega_r+i\gamma$ and eigenfunction $\delta\phi^l(r)$ has been determined numerically from Eq. (96) for the choice of density profile in Eq. (99). Typical results are illustrated in Table II, where ω_r and γ are tabulated versus $s=4\pi\hat{n}_bmc^2/B_0^2=\omega_{pb}^2(r=a)/\omega_c^2$ for mode number $l=2$, and s in the range $0.48\le s\le1$. For $s\lesssim0.45$, it is found that the system is *stable* ($\gamma=\mathrm{Im}\omega\le0$). For $s=0.48$, the onset of instability occurs for $l=2$ (Table II). On the other hand, as s is increased to $s=1$ it is found that the instability bandwidth increases to include $l=2,3,4$, and that maximum growth for $s=1$ occurs for $l=2$, where $\mathrm{Im}\omega/\omega_c=0.0977$ and $\mathrm{Re}\omega/\omega_c=0.248$.

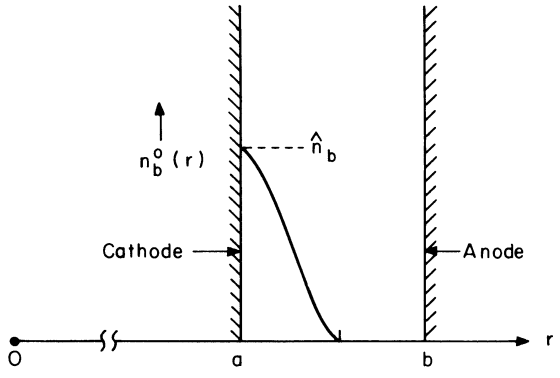

FIG. 7. Plot of $n_b^0(r)$ versus r for the bell-shaped density profile in Eq. (99).

TABLE II. $\mathrm{Re}\omega/\omega_c$ and $\mathrm{Im}\omega/\omega_c$ versus $s=4\pi\hat{n}_b mc^2/B_0^2$ [Eq. (96)] for $b/a=3$, $r_b/a=2$, and $l=2$ for the bell-shaped density profile in Eq. (99).

	$l=2$; $b/a=3$; $r_b/a=2$	
s	$\mathrm{Re}\omega/\omega_c$	$\mathrm{Im}\omega/\omega_c$
0.48	0.074	0.005×10^{-1}
0.5	0.077	0.012×10^{-1}
0.6	0.089	0.067×10^{-1}
0.7	0.101	0.178×10^{-1}
0.8	0.117	0.397×10^{-1}
0.9	0.156	0.779×10^{-1}
1.0	0.248	0.977×10^{-1}

It is useful to define a *resonant radius* r_s by the resonance condition

$$\omega_r - l\omega_E(r_s)=0 , \tag{100}$$

where $\omega_r=\mathrm{Re}\omega$ solves Eq. (96). It is readily shown for the two numerical examples analyzed in this section that r_s is located in the region where the electron density is nonzero (Figs. 8 and 9), i.e.,

$$a<r_s<r_b . \tag{101}$$

Unlike the simplified approximate eigenvalue equations analyzed in Secs. IV and V, it is important to recognize that the complete eigenvalue equation (96) provides collisionless dissipation even when $\partial\omega_{pb}^2/\partial r\,|_{r=r_s}=0$. This is evident from Table I, where the modes are weakly growing for the choice of rectangular density profile in Eq. (98) (where $\partial\omega_{pb}^2/\partial r\,|_{r=r_s}=0$ is trivially satisfied). The reason for this (negative) dissipation is readily traced to driving terms proportional to $\partial\omega_b^-/\partial r\neq0$ on the right-hand side of Eq. (96). It is precisely such terms that are neglected in the approximate eigenvalue equation (47) either by virtue of the assumptions $\omega_E(r)\ll\omega_c$ [Eq. (39)] or $|\omega-l\omega_E(r)|^2\ll\omega_c^2-\omega_{pb}^2(r)$ [Eq. (46)] used in obtaining Eq. (47).

To conclude this section, numerical plots of $n_b^0(r)$, $\omega_b^-(r)$, $\omega_r-l\omega_b^-(r)$, $\mathrm{Re}\delta\phi^l(r)$, and $\mathrm{Im}\delta\phi^l(r)$ versus r are presented in Figs. 8 and 9 for the two cases analyzed in Tables I and II, respectively. The parameters in Fig. 8 correspond to $s=0.5$ and $l=4$ (rectangular density profile) and in Fig. 9 to $s=1.0$ and $l=2$ (bell-shaped density profile).

C. Strong diocotron instability in a hollow electron beam

As an example in which Eq. (96) predicts strong diocotron instability, we now consider the hollow electron density profile specified by (Fig. 4)

$$n_b^0(r)=\begin{cases}0, & a\le r<r_b^- \\ \hat{n}_b=\text{const}, & r_b^-<r<r_b^+ \\ 0, & r_b^+<r<b\end{cases} \tag{102}$$

where the electron density ($\hat{n}_b$) is constant in the beam interior. Heretofore, the diocotron instability corresponding

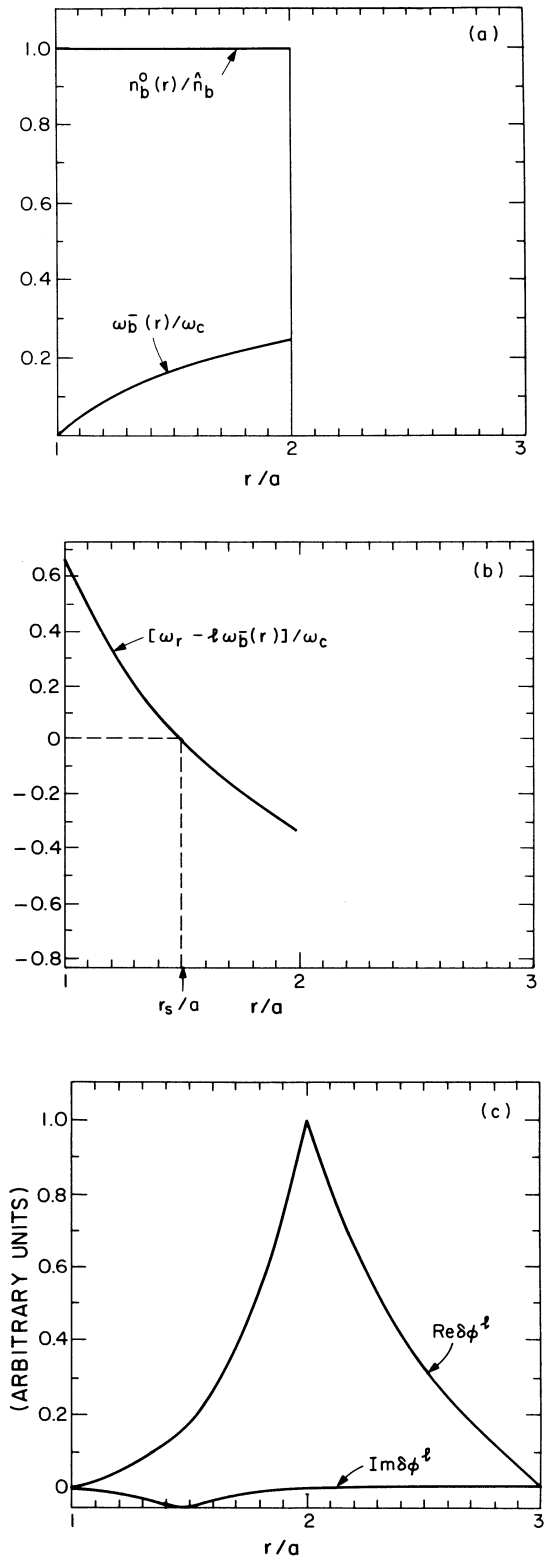

FIG. 8. (a) Plots of $n_b^0(r)/\hat{n}_b$ and $\omega_b^-(r)/\omega_c$ versus r/a for the rectangular density profile in Eq. (98) with $r_b/a=2$, $s=0.5$, and $b/a=3$ [case presented in Table I(a)]; (b) plot of $[\omega_r-l\omega_b^-(r)]/\omega_c$ versus r/a obtained from Eq. (96) for $l=4$ and $s=0.5$; (c) plots of $\mathrm{Re}\delta\phi^l$ and $\mathrm{Im}\delta\phi^l$ versus r/a obtained from Eq. (96) for $l=4$ and $s=0.5$.

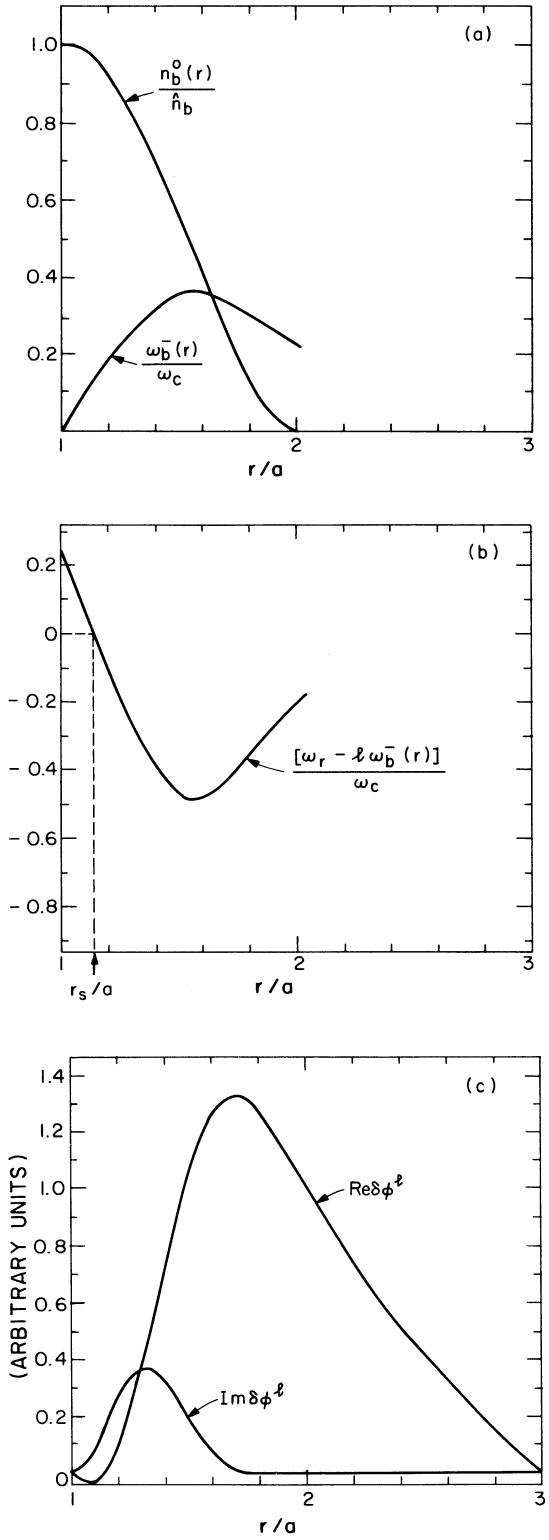

FIG. 9. (a) Plots of $n_b^0(r)/\hat{n}_b$ and $\omega_b^-(r)/\omega_c$ versus r/a for the bell-shaped density profile in Eq. (99) with $r_b/a=2$, $s=1.0$, and $b/a=3$ (case presented in Table II); (b) plot of $[\omega_r - l\omega_b^-(r)]/\omega_c$ versus r/a obtained from Eq. (96) for $l=2$ and $s=1.0$; (c) Plots of $\mathrm{Re}\delta\phi^l$ and $\mathrm{Im}\delta\phi^l$ versus r/a obtained from Eq. (96) for $l=2$ and $s=1.0$.

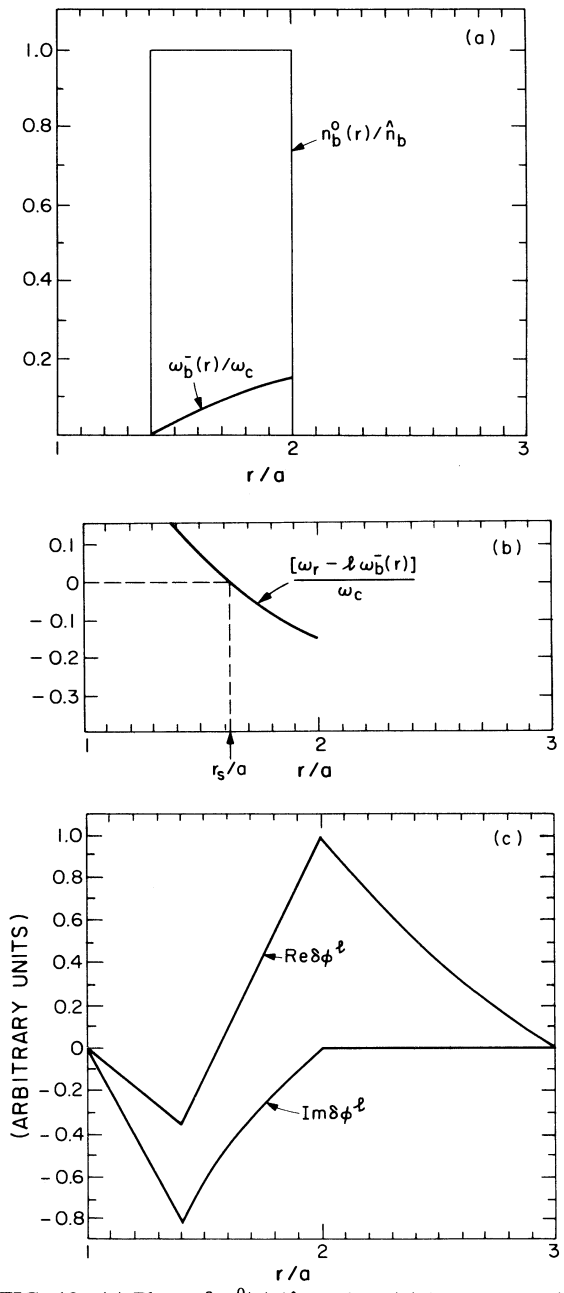

FIG. 10. (a) Plots of $n_b^0(r)/\hat{n}_b$ and $\omega_b^-(r)/\omega_c$ versus r/a for the hollow density profile in Eq. (102) with $r_b^-/a=7/5$, $r_b^+/a=2$, $b/a=3$, and $s=0.5$ [case presented in Table III(a)]; (b) plot of $[\omega_r - l\omega_b^-(r)]/\omega_c$ versus r/a obtained from Eq. (96) for $l=2$ and $s=0.5$; (c) plots of $\mathrm{Re}\delta\phi^l$ and $\mathrm{Im}\delta\phi^l$ versus r/a obtained from Eq. (96) for $l=2$ and $s=0.5$.

to the choice of density profile in Eq. (102) has been analyzed only for the low-density case ($s=\omega_{pb}^2/\omega_c^2 = 4\pi\hat{n}_b mc^2/B_0^2 \ll 1$) using a highly simplified (and approximate) form of the eigenvalue equation (96). In the present analysis, the complete eigenvalue equation (96) is solved numerically assuming $r_b^-/a=7/5$, $r_b^+/a=2$, and $b/a=3$. Typical results are illustrated in Table III, where $\omega_r=\mathrm{Re}\omega$ and $\gamma=\mathrm{Im}\omega$ are tabulated versus azimuthal mode number l for $s=0.5$ [Table III(a)] and $s=0.2$

TABLE III. $\mathrm{Re}\omega/\omega_c$ and $\mathrm{Im}\omega/\omega_c$ versus l [Eq. (96)] for $b/a=3$, $r_b^+/a=2$, $r_b^-/a=7/5$, and (a) $s=0.5$, and (b) $s=0.2$, for the hollow density profile in Eq. (102).

l	$\mathrm{Re}\omega/\omega_c$	$\mathrm{Im}\omega/\omega_c$
	(a) $s=4\pi\hat{n}_b mc^2/B_0^2=0.5$	
1	0.069	0.25×10^{-1}
2	0.144	0.59×10^{-1}
3	0.221	0.84×10^{-1}
4	0.301	0.86×10^{-1}
5	0.400	0.45×10^{-1}
	(b) $s=4\pi\hat{n}_b mc^2/B_0^2=0.2$	
1	0.025	0.095×10^{-1}
2	0.051	0.206×10^{-1}
3	0.079	0.282×10^{-1}
4	0.107	0.266×10^{-1}
5	0.151	0.013×10^{-1}

[Table III(b)] for the low-frequency branch that solves Eq. (96). Note from Table III that the instability growth rate $\gamma=\mathrm{Im}\omega$ is strongest at high density. Moreover, the growth rates in Table III (hollow density profile) are substantially larger than the growth rates in Table I (rectangular density profile in contact with the cathode). It should also be pointed out that the growth rate is reduced if the outer or inner conductors are brought closer to the surface of the electron plasma (i.e., smaller r_b^-/a or larger r_b^+/b). Finally, numerical plots of $n_b^0(r)$, $\omega_b^-(r)$, $\omega_r-l\omega_b^-(r)$, $\mathrm{Re}\delta\phi^l(r)$, and $\mathrm{Im}\delta\phi^l(r)$ versus r are shown in Fig. 10 for the case corresponding to $l=2$ and $s=0.5$ in Table III.

We have also solved the exact eigenvalue equation (96) numerically for the high-frequency branch. For all of the profiles and parameter ranges considered earlier in Sec. VI, it is found that the high-frequency branch is stable ($\gamma=\mathrm{Im}\omega\leq0$).

D. Summary of results and relationship to other work

To place the numerical results in Secs. VI B and VI C in the appropriate context, we summarize here the relationship to other work, including: exact analytic results[26] for the case of no internal conductor and a rectangular density profile that extends to $r=0$ (Sec. VI D 1); and comparison of the exact cylindrical eigenvalue equation (96) with its planar analog, which has been extensively analyzed by Buneman *et al.*[16] (Sec. VI D 2). Finally, we also summarize several conclusions on the qualitative influence of profile shape and location of conducting wall on stability behavior (Sec. VI D 3).

1. *Rectangular density profile extending to $r=0$*

For the specific case of no internal conductor and a rectangular density profile that extends to the origin [$a=0$ in Eq. (98)], the eigenvalue equation (96) can be solved analytically.[26] In this case, the angular rotation velocity

$$\omega_b^-=\frac{\omega_c}{2}[1-(1-2s)^{1/2}]=\text{const} \tag{103}$$

is independent of r [see Eq. (19)], where $s=\omega_{pb}^2/\omega_c^2=4\pi\hat{n}_b mc^2/B_0^2$. Moreover, the exact electrostatic dispersion relation for $k_z=0$ is given by[26]

$$0=1-\frac{\omega_{pb}^2[1-(r_b/b)^{2l}]}{2(\omega-l\omega_b^-)[(\omega-l\omega_b^-)-(\omega_c-2\omega_b^-)]} . \tag{104}$$

Equation (104) gives two stable solutions for ω, both with $\mathrm{Im}\omega=0$. For example, in the limiting case $b/r_b\to\infty$, the solutions for the real frequency ω are given by

$$\omega-l\omega_b^-=\omega_c-\omega_b^- , \tag{105}$$

and

$$\omega-l\omega_b^-=-\omega_b^- . \tag{106}$$

In the low-density regime ($s\ll1$), it follows that $\omega_b^-\simeq(s/2)\omega_c$, and Eq. (105) corresponds to a high-frequency branch with $\omega-l\omega_b^-\simeq\omega_c(1-s/2)$, whereas Eq. (106) corresponds to a low-frequency branch with $\omega-l\omega_b^-\simeq-(s/2)\omega_c$. On the other hand, in the high-density limit corresponding to cylindrical Brillouin flow ($2s=1$), Eqs. (105) and (106) reduce to $\omega-l\omega_c/2=\pm(\omega_c/2)$, both at relatively high frequencies.

To summarize, for a rectangular density profile extending to the origin ($a=0$), it follows that $\partial\omega_b^-/\partial r=0$ and $\partial\omega_E/\partial r=0$. Moreover, there are no solutions to $\mathrm{Re}\omega-l\omega_b^-(r)=0$ for any radius r_s within the electron density profile. Therefore, the stable behavior in this case is not surprising. Referring to the discussion and results in Secs. VI B and VI C, the reader will recall that the existence of nonzero shear and an "internal" resonant radius r_s were important prerequisites for existence of instability.

2. *Eigenvalue equation in planar geometry*

The cylindrical eigenvalue equation (96) undergoes some simplification in the limit of a planar diode with infinitely large aspect ratio, i.e., $a/(b-a)\to\infty$. In this case, we replace (r,θ) cylindrical coordinates by (x,y) Cartesian coordinates, and make the identifications: $r-a\to x$, $l/r\to k_y$, $\omega_b^-(r)r\to\omega_E(r)r\to V_y(x)=-cE_x^0(x)/B_0$, $l\omega_b^-(r)\to k_yV_y(x)$, and $\omega_E\to0$. In nondimensionless form, the planar limit of Eq. (96) [or Eq. (34) with $k_z=0$] reduces to

$$\frac{\partial}{\partial x}\left[\left[1-\frac{\omega_{pb}^2(x)}{[\omega-k_yV_y(x)]^2-[\omega_c^2-\omega_{pb}^2(x)]}\right]\frac{\partial}{\partial x}\delta\phi\right]-k_y^2\left[1-\frac{\omega_{pb}^2(x)}{[\omega-k_yV_y(x)]^2-[\omega_c^2-\omega_{pb}^2(x)]}\right]\delta\phi$$
$$=\frac{k_y\delta\phi\omega_c}{[\omega-k_yV_y(x)]}\frac{\partial}{\partial x}\left[\frac{\omega_{pb}^2(x)}{[\omega-k_yV_y(x)]^2-[\omega_c^2-\omega_{pb}^2(x)]}\right] . \tag{107}$$

Equation (107) is in agreement with the planar eigenvalue equation analyzed extensively by Buneman *et al.*[16]

Apart from the obvious difference between cylindrical and planar geometry, there are other important differences between Eqs. (96) and (107) related to finite aspect ratio. In particular, the gradient driving terms in Eq. (107) involve only $\partial\omega_{pb}^2/\partial x$ and $\partial V_y/\partial x$. On the other hand, it is clear from Eq. (96) that there are gradient terms proportional to $\partial\omega_E/\partial r$ *as well as* $\partial\omega_{pb}^2/\partial r$ and $\partial\omega_b^-/\partial r$. Indeed, as evident from Secs. VI B and VI C, for moderate aspect ratio the $\partial\omega_E/\partial r$ terms in Eq. (96) can make important contributions to stability behavior even when the density is uniform ($\partial\omega_{pb}^2/\partial r=0$) within the electron layer.

For the numerical examples in Tables I and II and Figs. 7–9 it should be noted that $(r_b-a)/a=1$, and therefore, cylindrical and finite-aspect-ratio effects are expected to play an important role. Nonetheless, it is informative to compare the growth rates in Table I with the short-wavelength planar estimate, $\mathrm{Im}\omega\sim(s/2)\omega_c\exp(-2/s)$, obtained by Buneman *et al.*[16] for a uniform density beam. For example, for $s=0.2$ [corresponding to Table I(b)], this estimate of growth rate[16] gives $\mathrm{Im}\omega\sim4.6\times10^{-6}\omega_c$, which is about 2 orders of magnitude smaller than the characteristic growth rate obtained numerically from Eq. (96) [Table I(b)]. Furthermore, we estimate $k_y(r_b-a)\sim(l/r_s)(r_b-a)=la/r_s$ for the case $(r_b-a)/a=1$. Therefore, because $k_y(r_b-a)$ is of order unity or somewhat larger for the range of unstable l values in Table I, it is *not* surprising that the short-wavelength (or long-wavelength) estimates[16] of growth rate in planar geometry do not apply to the circumstances analyzed in Secs. VI B and VI C, where cylindrical and finite-aspect-ratio effects are clearly important.

3. *Influence of profile shape and location of conducting wall*

The numerical results and analysis summarized in Secs. VI B and VI C are significant in several respects. Most important, the present work represents the first attempt to analyze the exact electrostatic eigenvalue equation (96) keeping the full complement of effects on stability behavior, including: cylindrical geometry and finite aspect ratio; finite $\omega_{pb}^2(r)/\omega_c^2$; dependence on profile shape; arbitrary frequency range, etc. While it is important not to make categorical generalizations based on the specific examples analyzed in Secs. VI B and VI C, several noteworthy tendencies and conclusions can be drawn from this analysis.

(i) For constant electron density, a conducting wall in contact with the plasma does not assure stability (Table I) although growth rates tend to be reduced relative to the case of a hollow annulus separated from the cathode (Table III).

(ii) A *decreasing* (bell-shaped) density profile in contact with the cathode [Eq. (99)] is more stable than a *constant* density profile [Eq. (98)], at least at low density. In particular, the bell-shaped profile in Eq. (99) is stable for $s=4\pi\hat{n}_b mc^2/B_0^2\lesssim0.48$ (Table II), whereas the constant density profile in Eq. (98) already exhibits (weak) instability for $s=0.2$ (Table I).

(iii) Although the numerical analysis shows that *decreasing* density profiles are qualitatively more stable than *flat* density profiles or *hollow* density profiles, it is clear that the stability theorem[17,25] discussed in Sec. IV is restricted to modest values of $\omega_{pb}^2(r)/\omega_c^2$ and to low frequencies with $|\omega-l\omega_b^-|^2\ll\omega_c^2-\omega_{pb}^2$. Indeed, the numerical analysis in Secs. VI B and VI C shows that the latter inequality is especially difficult to satisfy as $\omega_{pb}^2(r)/\omega_c^2$ is increased.

(iv) Finally, we reiterate that nonzero shear in $\omega_b^-(r)$ and $\omega_E(r)$, as well as the existence of an internal resonant radius r_s, where $\mathrm{Re}\omega-l\omega_b^-(r_s)=0$ within the plasma, are important prerequisites for the existence of instability for the examples discussed in Secs. VI B and VI C.

VII. CONCLUSIONS

In the present analysis we have made use of a *macroscopic* cold-fluid model (Secs. II and III) to investigate electrostatic stability properties of *nonrelativistic* sheared electron flow in a cylindrical diode with strong applied axial magnetic field $B_0\hat{e}_Z$. After reviewing the cold-fluid equilibrium properties, the linearized fluid-Poisson equation (25)–(27) were used in Sec. III to investigate stability behavior for electrostatic perturbations about a nonneutral cylindrical equilibrium characterized by (general) electron density profile $n_b^0(r)$ and self-consistent azimuthal velocity profile defined by $V_{\theta b}^0(r)=\omega_b^-(r)r$ [Eq. (15)]. For perturbations with complex oscillation frequency $\omega=\omega_r+i\gamma$, axial wave number k_z, and azimuthal harmonic number l, the linearized fluid-Poisson equations (29)–(33) were combined to give the eigenvalue equation (34). In Secs. IV and V, we investigated analytically stability properties associated with the approximate eigenvalue equations (43) and (47), assuming low-frequency flute perturbations with $k_z=0$, $|\omega-l\omega_E(r)|^2\ll\omega_c^2-\omega_{pb}^2(r)$, and $\omega_{pb}^2(r)<\omega_c^2$. This analysis included the derivation of a sufficient condition for stability (Sec. IV A), and the growth rate for weak resonant diocotron instability driven by a small density bump with $\partial\omega_{pb}^2/\partial r|_{r=r_s}>0$ (Sec. V B).

Finally, in Sec. VI we solved numerically the exact electrostatic eigenvalue equation (34) for $k_z=0$ and a wide range of electron density profiles $n_b^0(r)$ leading to weak and strong instability driven by velocity shear. In the numerical analysis of Eq. (34), no *a priori* restriction has been made to planar geometry[16,20,22–24] or to low electron density with $\omega_{pb}^2\ll\omega_c^2$.[15,17,18,20,21,25] Indeed, it is found that cylindrical effects, finite aspect ratio, and the strength of the equilibrium space-charge fields (as measured by ω_{pb}^2/ω_c^2) can have a large influence on stability behavior.

ACKNOWLEDGMENTS

This work was supported by Sandia National Laboratories and in part by the U.S. Office of Naval Research. It is a pleasure to acknowledge the benefit of useful discussions with Richard Aamodt.

[1]D. J. Johnson, G. W. Kuswa, A. V. Farnsworth, Jr., J. P. Quintenz, R. J. Leeper, E. J. T. Burns, and S. Humphries, Jr., Phys. Rev. Lett. 42, 610 (1979).
[2]J. P. Vandevender, J. P. Quintenz, R. J. Leeper, D. J. Johnson, and J. T. Crow, J. Appl. Phys. 52, 4 (1981).
[3]T. C. Genoni, M. R. Franz, R. B. Miller, and J. W. Poukey, J. Appl. Phys. 52, 2646 (1981).
[4]D. J. Johnson, E. J. T. Burns, J. P. Quintenz, K. W. Bieg, A. V. Farnsworth, Jr., L. P. Mix, and M. A. Palmer, J. Appl. Phys. 52, 168 (1981).
[5]R. C. Davidson (unpublished).
[6]R. C. Davidson (unpublished).
[7]R. C. Davidson and H. S. Uhm, Phys. Fluids 25, 2089 (1982).
[8]T. M. O'Neil, Phys. Fluids 23, 2216 (1980).
[9]R. C. Davidson, S. M. Mahajan, and H. S. Uhm, Phys. Fluids 19, 1608 (1976).
[10]R. C. Davidson, *Theory of Nonneutral Plasmas* (Benjamin, Reading, Mass., 1974), pp. 155—177.
[11]H. V. Wong, M. L. Sloan, J. R. Thompson, and A. T. Drobot, Phys. Fluids 16, 902 (1973).
[12]D. A. Hammer and N. Rostoker, Phys. Fluids 13, 1831 (1970).
[13]R. C. Davidson and N. A. Krall, Phys. Fluids 13, 1543 (1970).
[14]R. C. Davidson, Ref. 10, pp. 17—89.
[15]R. H. Levy, Phys. Fluids 8, 1288 (1965).
[16]O. Buneman, R. H. Levy, and L. M. Linson, J. Appl. Phys. 37, 3203 (1966).
[17]R. J. Briggs, J. D. Daugherty, and R. H. Levy, Phys. Fluids 13, 421 (1970).
[18]C. A. Kapetanakos, D. A. Hammer, C. D. Striffler, and R. C. Davidson, Phys. Rev. Lett. 30, 1303 (1973).
[19]B. L. Bogema and R. C. Davidson, Phys. Fluids 14, 1436 (1971).
[20]E. Ott and J.-M. Wersinger, Phys. Fluids 23, 324 (1980).
[21]M. E. Jones and M. A. Mostrom, J. Appl. Phys. 52, 3794 (1981).
[22]J. Swegle and E. Ott, Phys. Fluids 24, 1821 (1981).
[23]J. Swegle and E. Ott, Phys. Rev. Lett. 46, 929 (1981).
[24]R. C. Davidson and K. Tsang (unpublished).
[25]R. C. Davidson (unpublished).
[26]R. C. Davidson, Ref. 10, pp. 62—65.